Title:

# Strong Metal-Support Interactions of $TiO_2$ interface-loaded Pt constructed under different atmospheres for adjusting the hydrogen storage reaction performance of N-ethylcarbazole

*Zhengjian Hou[1], Ke Wu[2], Huijie Wei[1], Hua Chi[1], Yanyan Xi[1,3], Lishuang Ma[1,4], Xufeng Lin[1,4*]*

[1]College of Chemistry and Chemical Engineering, China University of Petroleum (East China), Qingdao, P. R. China, 266580

[2]Changqing Engineering Design Co.. Ltd., PetroChina Changqing Oilfield Company, Xi'an 710000, Shanxi, China

[3]Advanced Chemical Engineering and Energy Materials Research Center, China University of Petroleum (East China), Qingdao, P. R. China, 266580

[4]State Key Laboratory of Heavy Oil Processing, China University of Petroleum (East China), Qingdao, P. R. China, 266580

*Authors to whom correspondence should be addressed.

Email: hatrick2009@upc.edu.cn (X. Lin);

Tel (general office): +86-532-86984695.

# 1. Experimental Methods

## 1.1. Catalyst characterization

The platinum loading of the prepared samples was determined by dissolving the samples in aqua regia and using inductively coupled plasma photoemission spectrometry (ICP-OES).

X-ray diffraction (XRD) patterns of the prepared samples were recorded by an X'pert PRO MPD diffractometer (PANalytical) with a copper anode (Cu Kα, 40 kV, 40 mA, $\lambda$ = 0.1541 nm), $2\theta$ = 4.5-90°, in steps of 0.0167°.

The adsorption isotherms for $N_2$ were performed at 77 K using an ASAP 2020 physisorption instrument.

The $H_2$-TPD curves of the samples were obtained with a chemisorption instrument (FanTai 3010C). Firstly, 0.1g of sample was firstly loaded into a sample tube under $H_2$ atmosphere (40ml/min) at 350°C for 1h pretreatment to remove the passivation behavior of the metal particle surface. Next, the sample was treated at 300°C under Ar atmosphere (40ml/min) for 1h, cooled to room temperature, adsorbed $H_2$/AR (1:9) atmosphere (40ml/min) mixture for 1h, and programmed to increase the temperature to 0-600°C for desorption to collect the spectra. Measurements of static CO-pulse chemisorption were made on the Micromeritics AutoChem II 2920 to calculate the metal dispersion of platinum on titanium dioxide. One 200 mg sample was placed in a U-shaped quartz tube. The samples were pre-reduced at 350 °C for 3 h at 10% $H_2$/Ar flow (40 ml $min^{-1}$) to study the passivation behavior of the metals on the catalyst surface. Subsequently, the temperature was cooled to 30 °C under an Ar flow (40 ml $min^{-1}$) and then periodically injected with a pulsed stream of 10% CO/Ar until the catalyst was saturated with adsorption. The dispersion of the Pt NPs was then evaluated based on the consumption of CO.

Raman analysis was performed on a Jobin-Yvon Labram-010 Raman spectrometer at a wavelength of 532 nm (test range 100-2000 $cm^{-1}$).

The high-resolution transmission electron microscopy (HRTEM) images of the samples were taken with a JOEL JEM-2100 microscope.

X-ray photoelectron spectroscopy (XPS) spectra were performed using a hemispherical analyzer (111) with Al Kα1486.6 eV radiation (Thermo Escalab 250Xi) on a certain adsorbent. Photoelectron spectra were collected by a 150 W X-ray beam through energies of 100 and 0 eV. The spectra were collected by an X-ray beam of 150 W with a diameter of 400 μm. The samples were discharged at room temperature at a pressure of 10-8 Pa. The peaks were positioned from an external reference of 284.9 eV for the C1s peak and corrected for charge effects.

In situ diffuse reflectance infrared Fourier transform (DRIFT) spectra were measured using a Thermo Nicolet Nexus spectrometer equipped with a CdTe detector cooled by useful liquid nitrogen. Each DRIFT spectrum was collected using 128 scans with a resolution of 4 cm-1. The specific steps of the CO- DRIFT measurement spectra were as follows, first a certain 10 mg sample was placed in a quartz crucible and then loaded into a ZnSe window. Next, the samples were pretreated in H2 atmosphere (40 ml/min) at 300 °C for 1 h before adsorption of CO After cooling the samples to room temperature in N2 atmosphere (40 ml/min), the background spectra of the samples were collected. Subsequently, CO atmosphere (40 ml/min) was introduced into the spectral chamber for 30 min to saturate the carbon monoxide adsorption, and then the chamber was continuously purged with $N_2$ atmosphere (40 ml/min) until the IR signal of the sample stopped changing. Finally, CO-DRIFT spectra were collected.

Before performing 12H-NEC-DRIFT measurements, 12H-NEC is absorbed on the sample for 12 hours at room temperature. Physically adsorbed 12H-NEC was desorbed for 24 hours at 150°C under vacuum. Similarly, background spectra were collected using the same samples without adsorbed 12H-NEC.

**1.2. NEC hydrogenation and 12H-NEC dehydrogenation reaction test**

The hydrogenation of NEC was performed by adding catalyst (0.3 g) and NEC (3 g) in a high temperature stainless steel reactor at 6 MPa with 1200 rpm for 2 h at 130-170°C. Furthermore, a commercial 5% Ru-$Al_2O_3$ catalyst was used for hydrogenation under the same conditions for 5h to obtain 12H-NEC, a product of complete hydrogenation of NEC.

Similarly, the dehydrogenation reaction was performed in a high temperature stainless steel reactor with the addition of catalyst (0.3 g) and 12H-NEC (3 g) at 150-180 °C for 6 h at atmospheric pressure with 1200 rpm. The hydrogenation and dehydrogenation products were analyzed for product composition and product content by GC (Agilent) and elemental analyzer (Multi). Hydrogen release is recorded with an electronically displayed flow recorder (Figure S1).

**Figure S1 Experimental equipment physical diagram**

### 1.3. Theoretical calculations

All calculations were performed with the Vienna Ab initio Simulation Package (VASP)[1,2], based on the DFT method and the generalized gradient approximation, using the generalized functions (GGA-PBE) of Perdew et al[3–5]. The electron-ion interaction is described by the projector-enhanced wave (PAW) method using a plane wave basis set with a cutoff energy of 400 eV[6]. In the calculation, the top atomic layer of $TiO_2$ (101) is allowed to relax, while the bottom atomic layer of the slab is fixed. The Brillouin zone is integrated using a 3 × 3 × 1 Monkhorst-Pack grid. The low end of the sample model is elevated by 1 Å vacuum zone and the sample surface is separated by a vacuum region of 15 Å. The structural optimization is performed with a termination criterion of 0.02 eV/Å atomic force and the energy threshold for determining the self-consistency of the electron density is set to $10^{-6}$ eV. Transition state (TS) search was performed at the same level of theory using the CI-NEB The transition state (TS) search was performed at the same level

of theory by the method[7]. All models were optimized and screened to obtain the most stable structure.

Calculation of the binding energy (*BE*) of all intermediates on the sample surface is as follows:

$$BE_{ad} = E_{nH-NEC/surface} - E_{nH-NEC} - E_{surface}$$

where $E_{\text{nH-NEC/surface}}$ is the total energy of the intermediate and the surface, $E_{\text{n-NEC}}$ is the total energy of nH-NEC (n=0,4,6 and 12) in the gas phase, and $E_{\text{surface}}$ is the total energy of the sample surface.

For Pt-loaded P25, the $TiO_2$ (101) surface is the most stable and has the most dominant exposed crystalline surface and the lowest surface energy (HTEM results and XRD convolutions), and therefore it is generally chosen as a representative surface for experimental and theoretical studies. Therefore, the $TiO_2$ (101) surface was chosen to model the Pt/$TiO_2$ samples and represented by a four-layer (4 × 4) unit cell. In order to investigate the effect of surface Pt clusters on the activity and selectivity of 12H-NEC dehydrogenation and its inverse hydrogenation reaction, metal clusters consisting of five Pt atoms were added to the topmost layer, and the $TiO_2$ (101) interface was modeled with the results of XPS and Raman tests. A vacuum layer of 15 Å was added perpendicular to the direction in order to avoid surface periodic interactions. During the optimization process, the top metal clusters were allowed to relax together with the surface $TiO_2$ and the bottom layer was fixed. The specific structure is shown in the supporting information Figure S2.

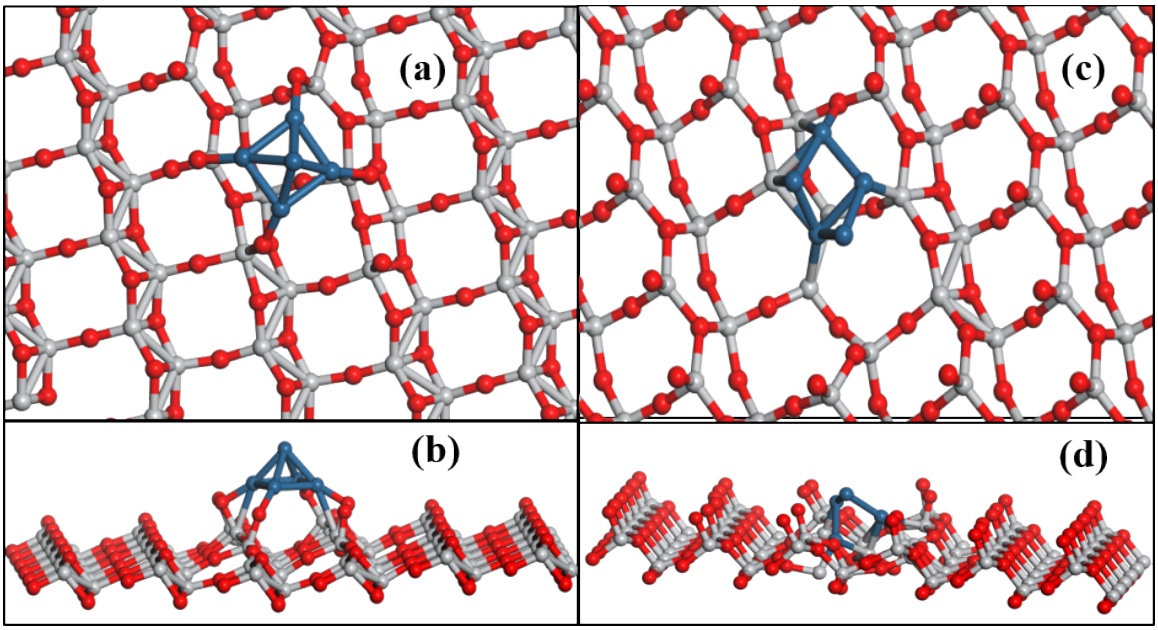


**Figure S2. Specific optimization models TR-$TiO_2$ (a, b) and RT-$TiO_2$ (c, d), respectively.**

The catalytic performance of a catalyst for NEC/12H-NEC hydrogenation/dehydrogenation reaction is calculated and the value of TOFs is calculated based on the conversion of a certain amount of cinnamaldehyde per second per platinum atom, as shown in the following equation:

$$S_{(NEC)} = \frac{C_{(NEC)}}{C_{(12H-NEC)_0} - C_{(12H-NEC)}} * 100\%$$

$$S_{(12H-NEC)} = \frac{C_{(12H-NEC)}}{C_{(NEC)_0} - C_{(NEC)}} * 100\%$$

Where "()" and "$()_0$" represent the concentration of a substance in the product and initial reactant, respectively.

$k_1$, $k_2$ and $k_3$ represent rate constants for the three basic reactions and are calculated as follows:

$$In_{12H-NEC} - In_{12H-NEC0} = k_1 t$$

$$In_{8H-NEC1} - In_{8H-NEC0} = k_2 t$$

$$In_{NEC1} - In_{NEC0} = k_3 t$$

$$TOFs = \frac{rAC}{n_{total} \times D}$$

rAc is the amount of reactant converted per second per gram of catalyst in mol/g·s, $n_{total}$ is the total substance of the metal, and D is the metal dispersion in .

$$In_{12H\text{-}NEC1} - In_{12H\text{-}NEC0} = k_1 t$$

$$In_{8H\text{-}NEC1} - In_{8H\text{-}NEC0} = k_2 t$$

$$In_{4H\text{-}NEC1} - In_{4H\text{-}NEC0} = k_3 t$$

Where nH-NEC0 represents the initial concentration of reactants, $mol \cdot ml^{-1}$; nH-NEC1 represents the concentration of reactants, $mol \cdot ml^{-1}$; $k_1$; $k_2$; $k_3$ represent the reaction rate constants; t is the reaction time, min.

## 2. Results and discussion

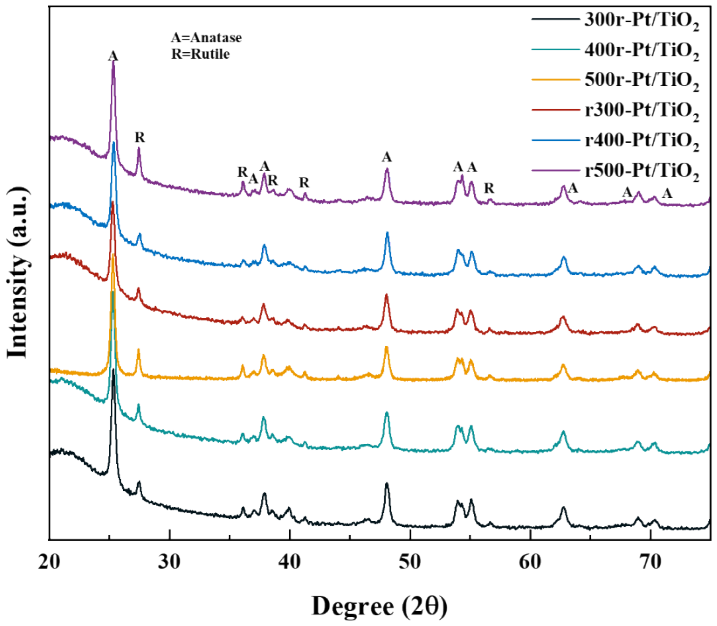


**Figure S3. Powder XRD patterns of the samples. Peaks characteristic of anatase and rutile are labeled as A and R, respectively.**

The XRD profiles of the prepared samples are shown in Figure S3. And the diffraction peaks were calibrated according to the standard database JCPDS (anatase phase No. 21-

1272 and rutile phase No. 21-1276). The 2θ characteristic peaks at 25.4, 37.8, 48.0, and 54.1° are attributed to the anatase phase and correspond to the (101), (004), (200), and (211) crystal planes, respectively. In addition, peaks at 27.4, 35.1, and 35.7° correspond to the (110), (211), and (101) crystal faces of the rutile phase, respectively. The XRD patterns of all the samples are characterized by peaks of anatase and rutile phases, which are typical of the P25 structure, without significant changes in the peak positions of $TiO_2$, indicating that metal loading and high temperature treatment do not affect the intrinsic structure of $TiO_2$. At 39.5° and 46.4°, two weak reflection peaks of Pt metal are observed, which can be identified as the (111) and (200) reflection peaks of Pt metal cluster, respectively. In addition, according to the Scherrer equation, the crystal size (in nanometers) on the catalyst can be calculated from the XRD data by the diffraction peaks of anatase (101) and rutile (110). Table S1 shows the crystal size values of anatase and rutile in the samples.

**Table S1. Crystal size values of anatase and rutile in the prepare samples**

| | crystal size (nm) | |
|---|---|---|
| sample | Anatase (2θ = 25.4°) | Rutile (2θ = 27.4°) |
| 300r-Pt/$TiO_2$ | 18.1 | 29.0 |
| 400r-Pt/$TiO_2$ | 18.7 | 30.2 |
| 500r-Pt/$TiO_2$ | 18.9 | 29.6 |
| r300-Pt/$TiO_2$ | 18.3 | 29.6 |
| r400-Pt/$TiO_2$ | 18.6 | 29.9 |
| r500- Pt/$TiO_2$ | 18.7 | 29.9 |

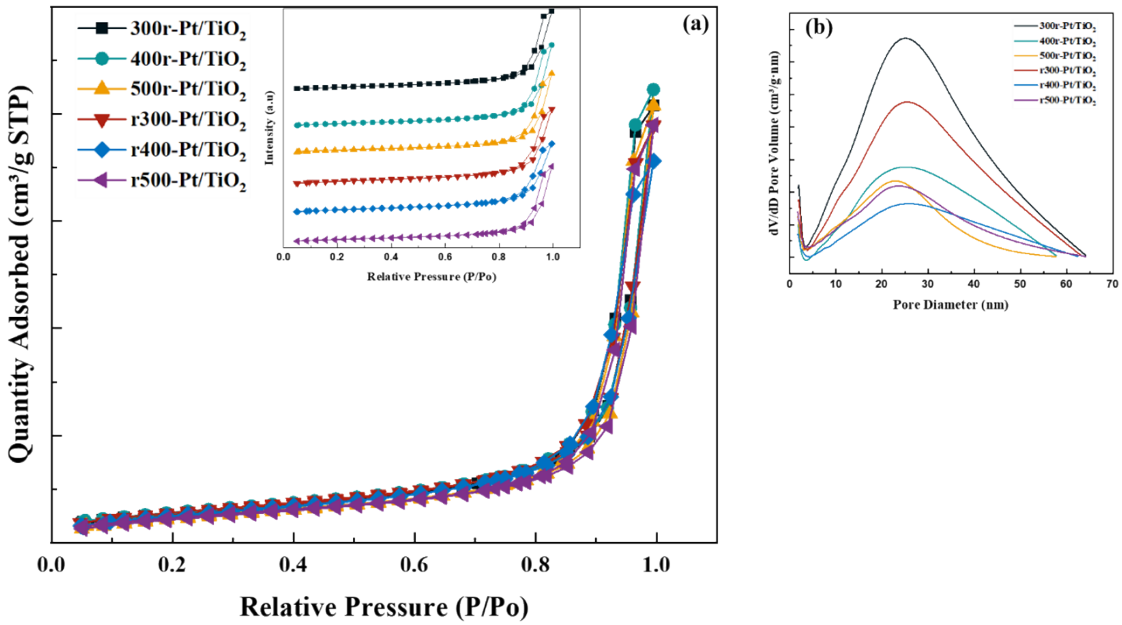


**Figure S4. $N_2$ adsorption-desorption isotherms (a), and Pore size distribution calculated from the adsorption branch of the isotherms (b) of the prepared samples at 77 K.**

According to the XRD spectra (see Figure S3), $TiO_2$ was mainly characterized by anatase (101) and rutile (110), while the exposed surfaces of Pt clusters were mainly Pt (111) as analyzed in the supporting information[8,9]. $N_2$ adsorption-desorption isotherms at 77 K for the prepared samples are shown in Figure S4a. It can be clearly seen that all the samples in this study are characterized by type IV isotherms (Figure S4b). Furthermore, the BET surface area, pore volume, and average pore size of the samples are given in Table S2. Combined with comparing the XRD spectra and BET curves of different samples, it is clearly seen that roasting did not affect the intrinsic properties of the samples.

**Table S2. BET surface area, pore volume of and average pore diameters of samples calculated from the 77 K $N_2$ adsorption-desorption isotherms**

| sample | SBET (m2/g) | VTol (cm3/g) | Average pore size (nm) |
|---|---|---|---|
| 300r-Pt/TiO2 | 54.1 | 0.37 | 35 |
| 400r-Pt/TiO2 | 59.1 | 0.36 | 29 |
| 500r-Pt/TiO2 | 54.5 | 0.32 | 25 |
| r300-Pt/TiO2 | 51.2 | 0.34 | 27 |
| r400-Pt/TiO2 | 53.4 | 0.37 | 25 |
| r500- Pt/TiO2 | 52.2 | 0.36 | 22 |

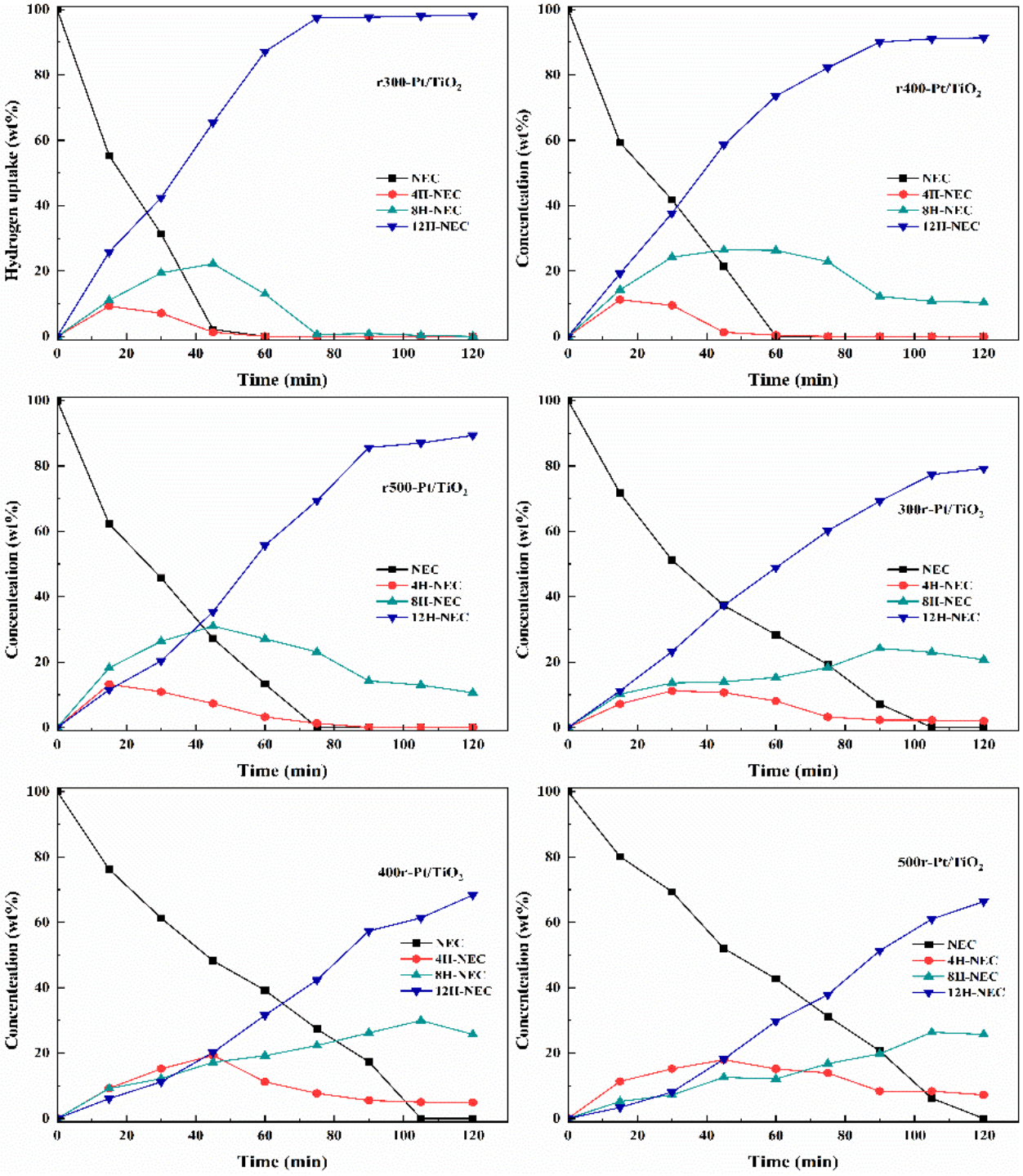


**Figure S5. The hydrogenation reaction products distribution of different samples**

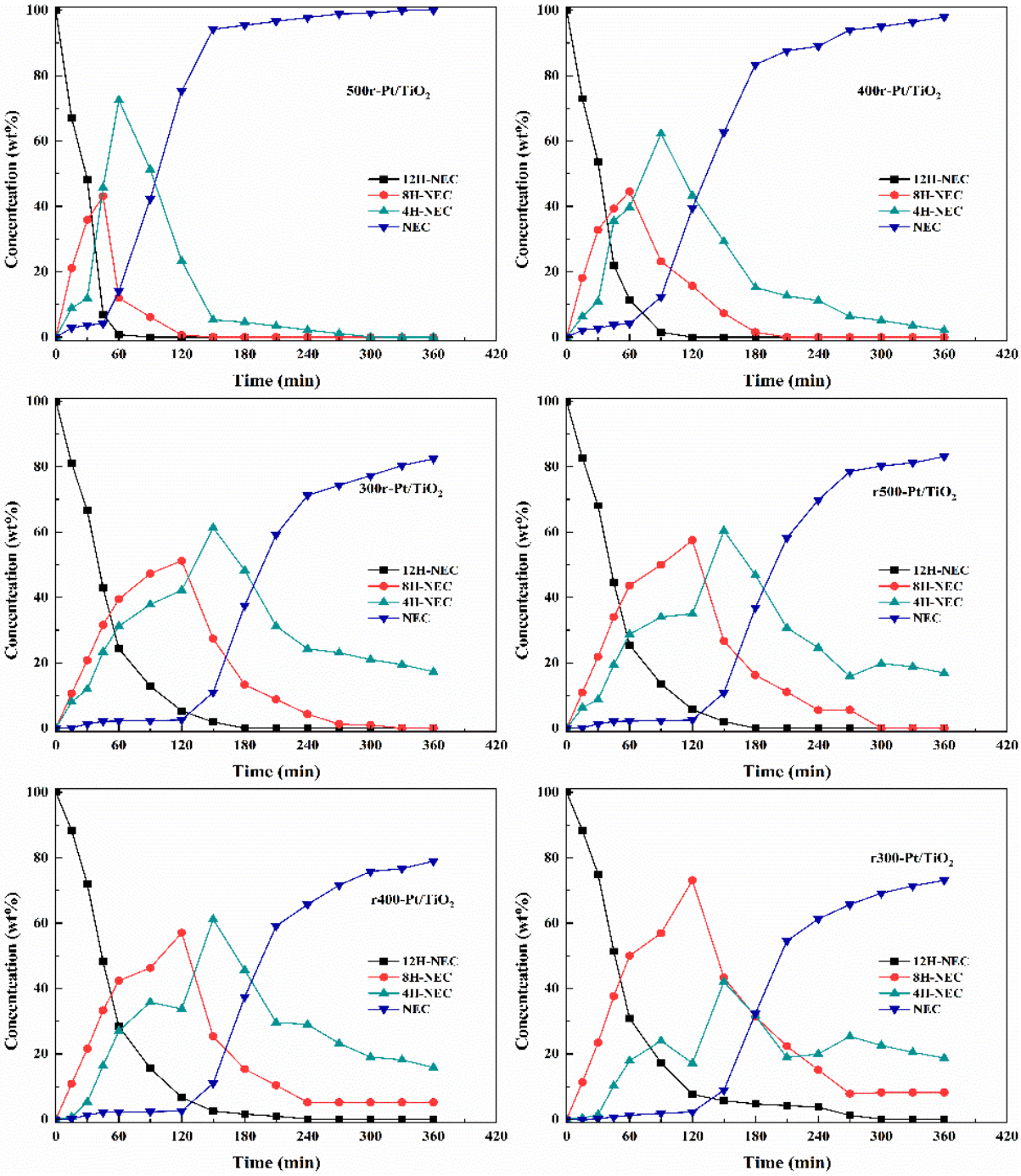


**Figure S6. The dehydrogenation reaction products distribution of different samples**

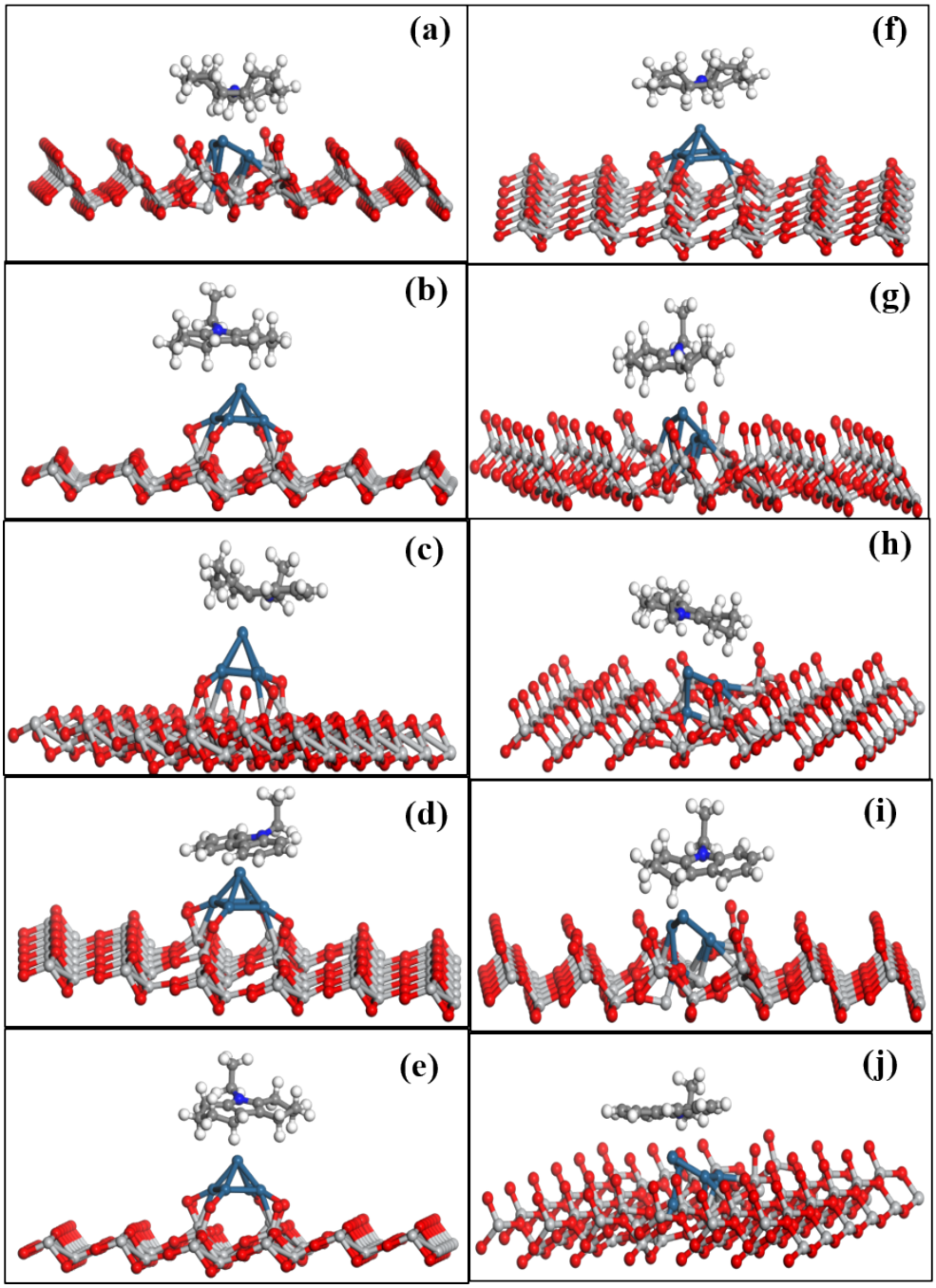


**Figure S7. Modeling of n-NEC adsorption on TR-$TiO_2$ (a-e) and adsorption on RT-$TiO_2$ (f-j), respectively.**

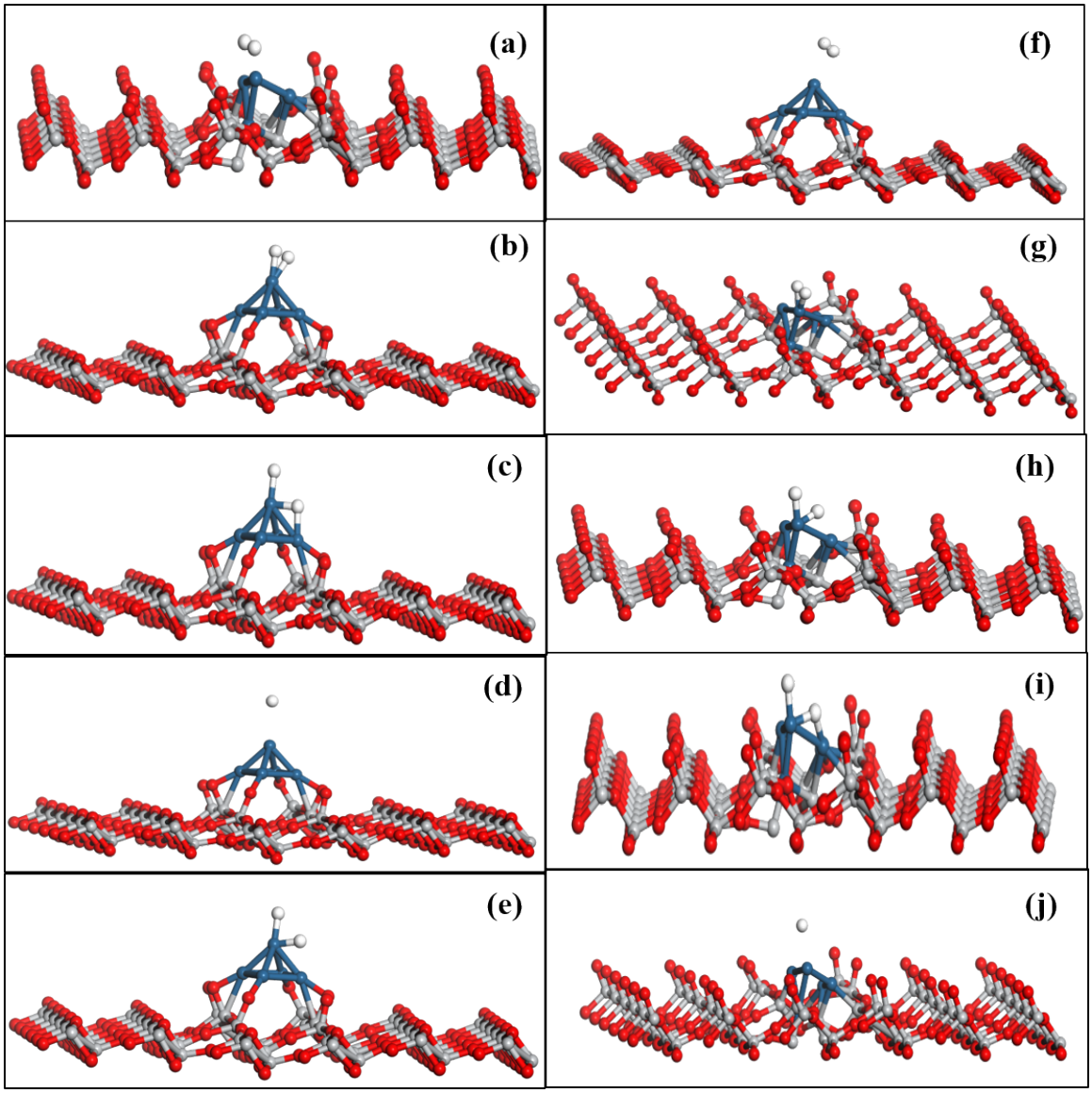


**Figure S8. Modeling of $H_2$ dissociation on TR-$TiO_2$ (a-e) and dissociation on RT-$TiO_2$ (f-j), respectively.**

**Table S3. Binding energies (eV) of 12H-NEC, 8H-NEC,6H-NEC 4H-NEC, and NEC on the surfaces of rT-Pt/$TiO_2$and Tr-Pt/$TiO_2$ were calculated by DFT**

| Species/surfaces | 12H-NEC | 8H-NEC | 6H-NEC | 4H-NEC | NEC |
|---|---|---|---|---|---|
| rT-Pt/TiO2 | -1.36 | -1.58 | -1.41 | -1.54 | -1.65 |
| Tr-Pt/TiO2 | -1.77 | -1.96 | -2.06 | -2.12 | -2.23 |

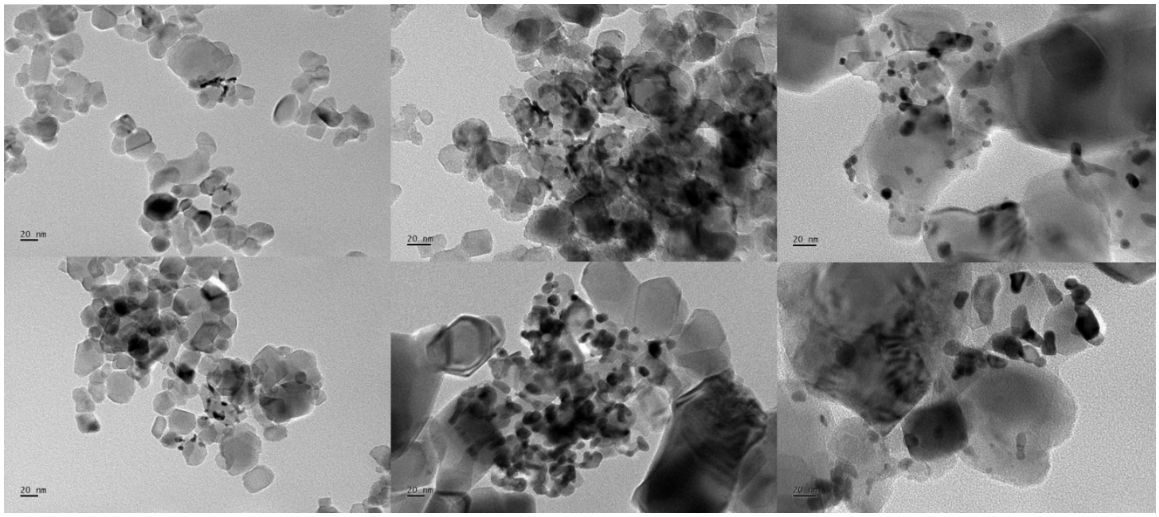

**Figure S9. HRTEM images of (a) r300-Pt/$TiO_2$, (b) r400-Pt/$TiO_2$, (c) r500-Pt/$TiO_2$, (d) 300r-Pt/$TiO_2$, (e) 400r-Pt/$TiO_2$, and (f) 500r-Pt/$TiO_2$(images at 20 nm scale)**

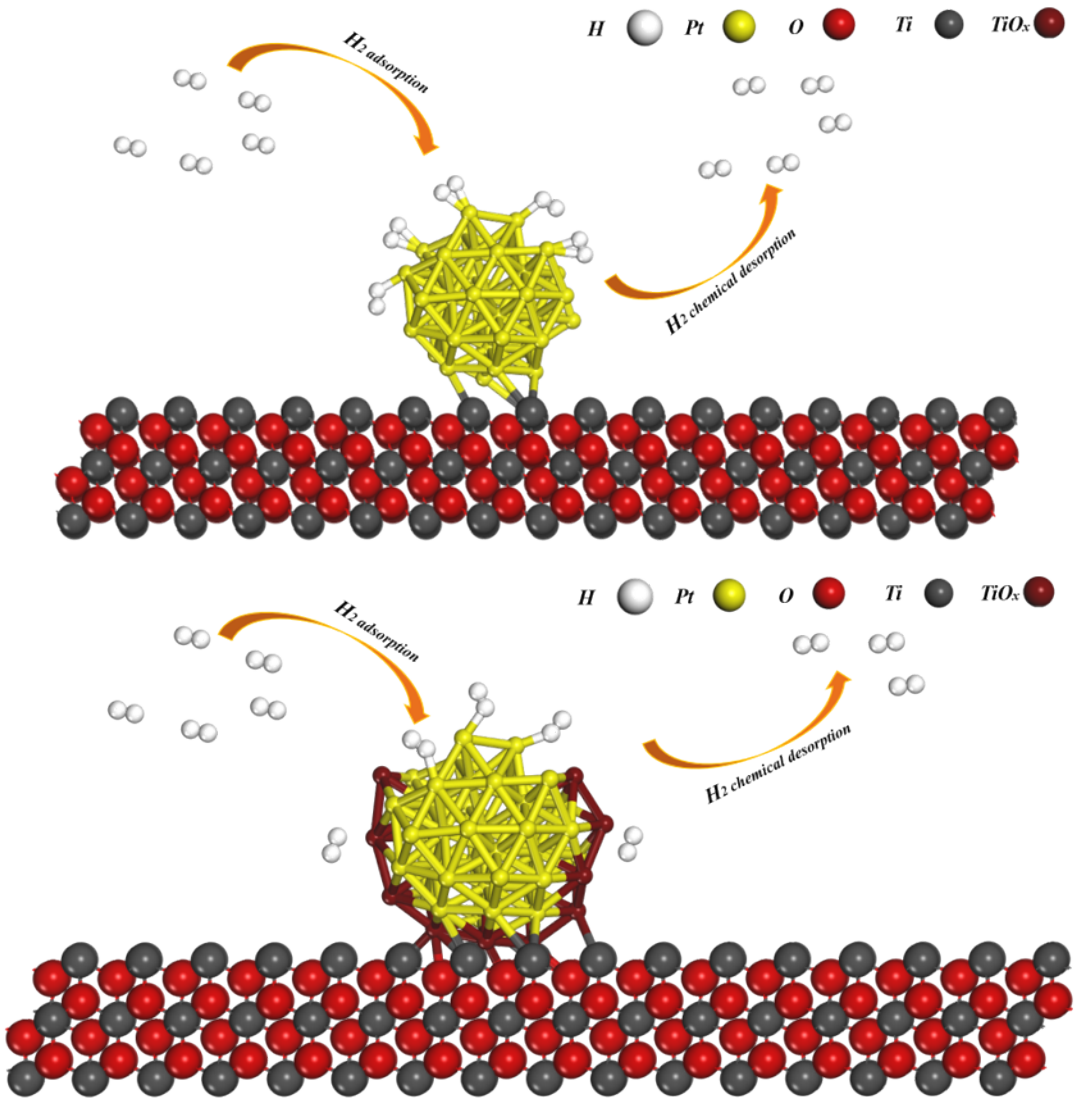


**Figure S10. Schematic diagram of the adsorption of small molecule gases by two different interfacial morphologies**

## References

1 G. Kresse and J. Furthmüller, *Computational Materials Science*, 1996, **6**, 15–50.

2 G. Kresse and J. Hafner, *Physical Review B*, 1993, **47**, 558–561.

3 J. P. Perdew, K. Burke and M. Ernzerhof, *Physical Review Letters*, 1996, **77**, 3865–3868.

4 J. P. Perdew, K. Burke and M. Ernzerhof, *Physical Review Letters*, 1997, **78**, 1396–1396.

5 J. P. Perdew, J. A. Chevary, S. H. Vosko, K. A. Jackson, M. R. Pederson, D. J. Singh and C. Fiolhais, *Physical Review B*, 1993, **48**, 4978.

6 D. Joubert, *Physical Review B - Condensed Matter and Materials Physics*, 1999, **59**, 1758–1775.

7 G. H. B. P. U. H. Jónsson, *J Chem Phys*, 2000, **113**, 9901–9904.

8 Z. T. Liu, C. X. Wang, Z. W. Liu and J. Lu, *Applied Catalysis A: General*, 2008, **344**, 114–123.

9 J. Yang, C. Tian, L. Wang and H. Fu, *Journal of Materials Chemistry*, 2011, **21**, 3384–3390.